

Energy Transfer from Multiple Excitons in a Perovskite Nanocrystal to Organic Dyes Revealed by Single-Particle Spectroscopy

Tetsuo Yamaguchi, Tomoya Fukumasu, Yukihide Ishibashi, and Sadahiro Masuo*



Cite This: *J. Am. Chem. Soc.* 2025, 147, 33944–33952



Read Online

ACCESS |



Metrics & More

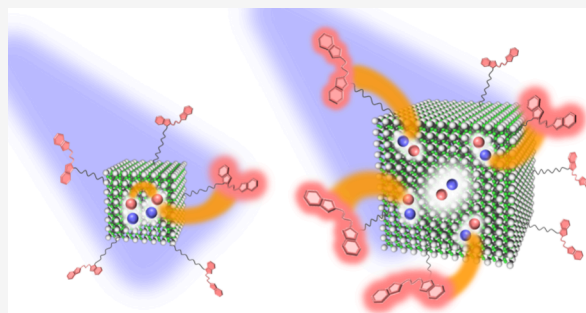


Article Recommendations



Supporting Information

ABSTRACT: Colloidal semiconductor quantum dots (QDs) can generate multiple excitons (MXs) within a single QD. Owing to their large absorption cross-section, efficient utilization of MX is anticipated for the development of light-harvesting systems. However, MXs typically undergo nonradiative decay via Auger recombination (AR). In this study, we investigated the possibility of energy transfer from the MXs in a single QD to multiple cyanine dyes (Cy3) adsorbed on the QD surface. Based on the linear relationship between the AR lifetime and QD volume, formamidinium lead bromide perovskite nanocrystals (PNCs) with three distinct size distributions were synthesized. Simultaneous measurements of emission photon correlations and individual pristine PNC sizes revealed that the probability of multiphoton emission increased in PNCs larger than 12 nm. This was attributed to a slowdown in the AR rate, which was evaluated by transient absorption spectroscopy. Subsequently, multiple Cy3 dyes were adsorbed onto the PNCs as energy acceptors to evaluate the transfer of energy from the MXs to multiple Cy3 dyes. Photon correlation measurements of Cy3 emission via energy transfer—induced by excitation of a single PNC—showed an increased probability of multiphoton emission in PNC-Cy3 systems with PNC sizes exceeding 12 nm. These findings indicate that multiple Cy3 dyes were excited and emitted via the energy transfer from MXs. Thus, we clearly demonstrate that energy transfer from MXs to multiple surface dyes is feasible using large-sized PNCs.



INTRODUCTION

Colloidal semiconductor quantum dots (QDs) are attractive materials owing to their remarkable optical properties, such as size-tunable photoluminescence (PL) wavelength, narrow PL line width, and high photodurability.^{1–5} With the recent development of lead halide perovskite nanocrystals (PNCs),^{6–10} QDs are being increasingly studied for optoelectronic applications. In addition to their PL properties, QDs—including PNCs—possess a large absorption cross-section, enabling them to readily absorb multiple photons and generate multiple excitons (MXs) within a single QD. The study of MXs is of great interest, as it opens new perspectives for designing photonic devices.^{11–15} Furthermore, multiphoton emission, which arises from the cascade emission as MXs decay to the ground state via the single exciton (SX) state,¹⁶ is associated with quantum entanglement of photons and can be utilized in quantum information technologies.¹⁷ However, MXs typically decay nonradiatively to SXs via Auger recombination (AR), which occurs at a faster rate than the radiative rate of MXs.^{18–22} As a result, excitons are inefficiently consumed through the AR. AR also induces PL blinking through a process known as Auger ionization.^{23–26} Consequently, the suppression of AR has been widely investigated to enable the effective use of excitons. The AR rate in QDs generally scales nearly linearly with the inverse of QD volume.^{18,20,27–30} Therefore, efficient strategies to suppress

AR in QDs include increasing the core volume or smoothing the confinement potential between the core and shell materials.^{31–34}

Another strategy to reduce the influence of AR without altering the QD structure is to enhance the radiative rate of MXs by coupling them with plasmonic nanostructures, thereby enabling MX emission before AR occurs.^{35–38} For example, interactions between QDs and plasmonic nanostructures—such as gold nanocubes,³⁹ silver-coated atomic force microscope cantilevers,⁴⁰ and others^{41–43}—have been shown to induce multiphoton emission from MXs. Through this approach, multiple photons can be extracted from MXs before their annihilation by AR, achieving conversion from MXs to multiple photons.

As a further step in mitigating the effects of AR, extracting the excitation energy from MXs to organic molecules adsorbed on the QD surface via energy transfer (ET)—effectively converting MX energy into multiple excited states in the

Received: June 30, 2025

Revised: August 22, 2025

Accepted: August 26, 2025

Published: September 8, 2025



molecules—is a promising approach. If such an ET is feasible, QDs can serve as light-harvesting moieties, paving the way for the development of various photosensitized systems. However, only a few studies have reported ET from MXs that is faster than AR.^{44–47} For instance, ET from the biexciton state in a CdSe QD to dye molecules adsorbed on the QD surface has been suggested based on PL lifetime measurements at the single-QD level.^{45,46} Additionally, femtosecond transient absorption measurements have revealed ET faster than AR.^{44,47} Recently, we investigated the possibility of ET from MXs in CdSe/ZnS core/shell QDs to a perylene bisimide derivative adsorbed on the QD, using photon correlation measurements.⁴⁸ This research indicated that ET from MXs was difficult to observe due to the faster AR in QDs compared to ET,⁴⁸ suggesting that a slower AR rate could enable ET from MXs to multiple dyes. The AR rate can be reduced by increasing the QD size. In this regard, PNCs are promising candidates because even those larger than their Bohr diameters retain “quantum dot-like” sharp PL spectra with high PL quantum yield (PLQY). In practice, we demonstrated—using photon correlation measurements on single PNCs—that the AR rate decreases and multiphoton emission increases with PNC volume.³⁴ Therefore, efficient utilization of MXs is expected via ET from larger PNCs to adsorbed organic dyes.

In this work, we employed formamidinium lead bromide (FAPbBr₃) PNC-cyanine 3 dye (Cy3) linkage systems (referred to as PNC-Cy3 systems) to investigate the dependence of ET from MXs on PNC size. In these systems, ET follows Förster-type fluorescence resonance energy transfer (FRET),^{49,50} which allows for a simplified interpretation of size-dependent ET effects. FAPbBr₃ PNCs with three distinct size distributions were synthesized, and Cy3 dyes were adsorbed onto the PNCs to evaluate the size dependence of ET. First, ET from the PNCs to Cy3 was confirmed in solution at the ensemble level. Next, the ET was examined at the single-PNC level. Initially, the adsorption of multiple Cy3 dyes onto individual PNCs was confirmed by analyzing the emission photon statistics of Cy3 upon direct excitation. Then, the possibility of ET from MXs in PNCs to multiple Cy3 dyes was investigated by measuring the emission photon statistics of Cy3 under the selective excitation of the PNCs. In the case of small PNC-Cy3 systems, single-photon emission from Cy3 was observed via ET from the PNC to the dye. As the PNC size increased, the emission photon statistics of Cy3 transitioned from single-photon to multiphoton emission, suggesting successful ET from MXs in a single PNC to multiple Cy3 dyes adsorbed on its surface.

RESULTS AND DISCUSSION

Characterization of PNC. To observe the morphology and size of the synthesized PNCs with three size distributions, transmission electron microscopy (TEM) observation was performed (Figure 1a–c). The TEM images indicated the preparation of cubic-shaped crystals in all three PNC samples. The edge lengths, L_{PNC} , of the small-, middle-, and large-sized PNCs were estimated to be 7.9 ± 0.6 nm (referred to as s_{PNC}), 12.1 ± 1.2 nm (referred to as m_{PNC}), and 15.9 ± 1.0 nm (referred to as l_{PNC}), respectively (Figure 1d).

Absorption and PL spectra of the PNCs in toluene are shown in Figure S1 in the Supporting Information. The PL peaks of the PNCs were 520 nm for s_{PNC} , 533 nm for m_{PNC} , and 535 nm for l_{PNC} . The increase in the PL peak wavelength with increasing PNC size is attributed to the quantum

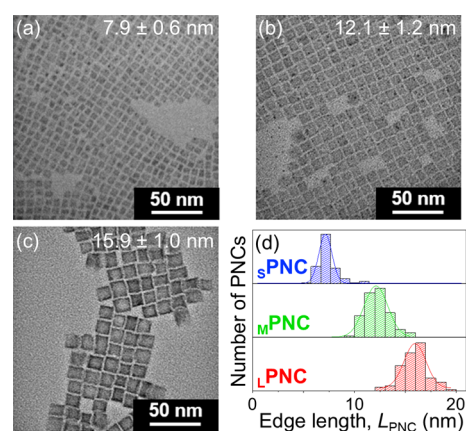


Figure 1. TEM images of s_{PNC} (a), m_{PNC} (b), and l_{PNC} (c) and size distributions of the PNCs (d).

confinement effect. The obtained sizes and PL peaks are comparable to previously reported values.⁵¹ The PLQYs were 81, 82, and 68% for s_{PNC} , m_{PNC} , and l_{PNC} , respectively.

Estimation of Förster Radii. As an acceptor dye, Cy3 with a carboxy group as an adhesion moiety to PNCs (Figure 2

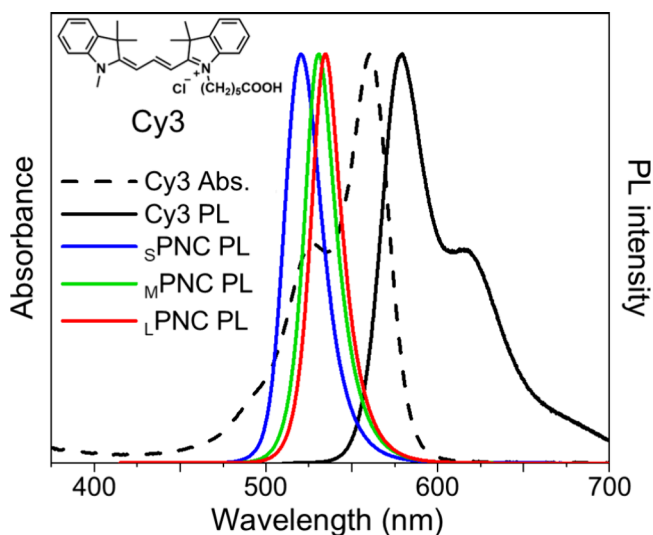


Figure 2. Absorption (dashed line) and PL (black solid line) spectra of Cy3 in toluene with PL spectra of the PNCs dispersed in toluene (colored solid lines). Inset: molecular structure of Cy3.

inset) was used. Absorption and PL spectra of Cy3 are shown in Figure 2, along with the PL spectra of the PNCs. The spectral overlap integral, $J(\lambda)$, between the PL spectra of the PNCs and the absorption spectrum of Cy3 was estimated to be 6.23×10^{15} , 7.66×10^{15} , and 8.14×10^{15} $\text{M}^{-1} \text{cm}^{-1} \text{nm}^4$ for $s_{\text{PNC-Cy3}}$, $m_{\text{PNC-Cy3}}$, and $l_{\text{PNC-Cy3}}$, respectively. Using these values, the Förster radii (R_0) were calculated as 5.90, 6.12, and 5.99 nm for $s_{\text{PNC-Cy3}}$, $m_{\text{PNC-Cy3}}$, and $l_{\text{PNC-Cy3}}$, respectively (details in the Supporting Information). To adsorb Cy3 onto the PNC surface, Cy3 and the PNCs were mixed in toluene at various $[\text{Cy3}]/[\text{PNCs}]$ ratios. The resulting solutions were then used for the measurements.

Evaluation of ET in Solution. To confirm ET from the PNCs to Cy3, absorption, PL, and excitation spectra of PNC-Cy3 systems were measured in toluene at various $[\text{Cy3}]/[\text{PNCs}]$ ratios while fixing $[\text{PNCs}]$ at 2.5×10^{-9} M (Figure 3).

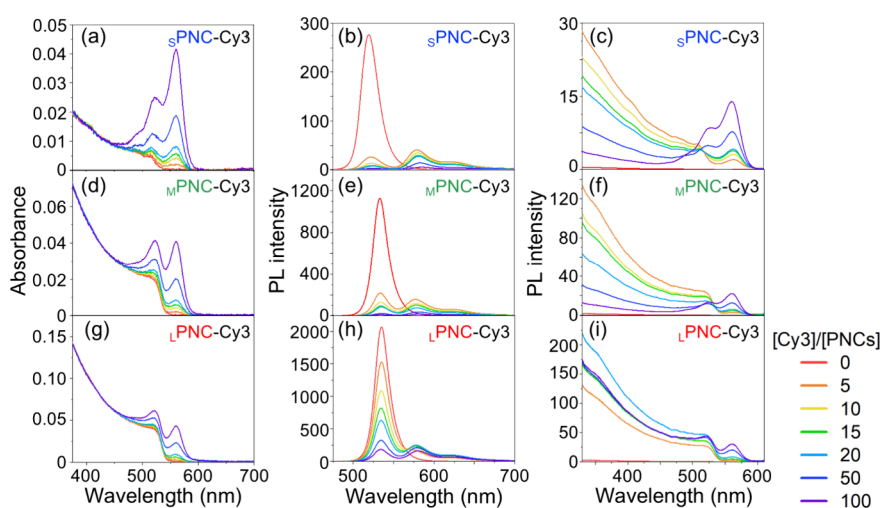


Figure 3. Absorption (a, d, g), PL (b, e, h), and excitation spectra (c, f, i) of *s*PNC-Cy3 (a–c), *m*PNC-Cy3 (d–f), and *l*PNC-Cy3 (g–i) dispersed in toluene at various [Cy3]/[PNCs] ratios. The PL spectra were measured by 405 nm excitation. The excitation spectra were measured by monitoring the PL of Cy3 at 620 nm.

In absorption spectra (Figure 3a,d,g), the absorbance derived from the PNCs increased with size, because of the size-dependent molar absorption coefficients (details in the Supporting Information). The spectra were superpositions of those of Cy3 and the PNCs (Figure S1) without a spectral shift, suggesting that Cy3 adsorbed on the PNCs without significant electronic interaction.

Figure 3b,e,h shows PL spectra measured with excitation at 405 nm. PL from Cy3 was observed in the presence of PNCs, accompanied by a decrease in PNC PL. Because Cy3 has negligible absorption at 405 nm (Figure 2), no PL was observed in a Cy3 toluene solution alone (Figure S5). Thus, the appearance of Cy3 PL and the decrease in the PNC PL suggest ET from PNCs to Cy3. At higher [Cy3]/[PNCs] ratios, Cy3 PL decreased and slightly red-shifted, implying intermolecular interactions among the adsorbed dyes. Figure 3c,f,i shows excitation spectra of the PNC-Cy3 systems monitored at 620 nm, where only Cy3 PL appears. The PL by Cy3 increased with [Cy3]/[PNCs], and even in the absence of PNC PL at 620 nm, the contribution of PNC absorption below 530 nm supports the ET to Cy3. PL intensity in this region increased and then decreased with [Cy3]/[PNCs], supporting intermolecular Cy3 interactions. ET was further confirmed by shortened PNC PL lifetimes and rise components in Cy3 PL decay (details in the Supporting Information).

From the PL quenching of the PNCs, ET efficiency (E_{ET}) was estimated as $E_{ET} = \frac{I_0 - I}{I_0} \times 100$, where I and I_0 are the PL intensity of the PNCs with and without Cy3, respectively. The estimated E_{ET} values are shown in Figure 4, alongside theoretical ET efficiency (E_{FRET}) based on FRET theory, considering the distribution of donor–acceptor distance that depends on the adsorption positions of dyes on PNCs (details in the Supporting Information). The E_{ET} values fall within the range of E_{FRET} but are relatively higher. This result suggests that the ET occurs preferentially to Cy3 dyes located at shorter donor–acceptor distances or that other processes in addition to ET, such as electron transfer to Cy3, are involved. E_{ET} values estimated from PL lifetime measurements also matched E_{FRET} (Figure S9), indicating that ET from PNCs to Cy3 occurred via FRET.^{50–52} To further investigate ET from MX in

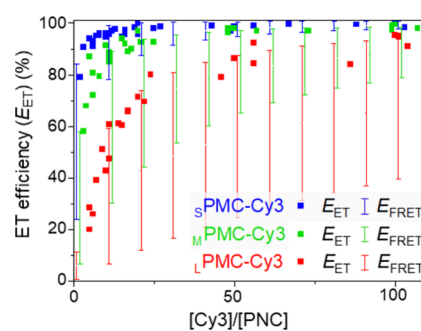


Figure 4. ET efficiencies (E_{ET}) of PNC-Cy3 systems estimated from PL quenching of PNCs at various [Cy3]/[PNCs] ratios in toluene (dots), along with E_{FRET} calculated from the FRET theory (solid lines).

PNCs to multiple Cy3 dyes, PL properties were examined at the single PNC-Cy3 level.

Emission Photon Statistics of Single PNCs with Different Sizes. Before the evaluation of ET in the single PNC-Cy3 systems, the correlation between emission photon statistics and PNC size in single pristine PNCs was investigated. The number of emitted photons per laser pulse, $\langle N_p \rangle$, from a single PNC depends on the PNC size, with larger PNCs showing greater $\langle N_p \rangle$ due to slower AR.⁵⁰

To examine this correlation, PL spectra and photon correlation were obtained by detecting PL from single pristine PNCs using two avalanche photodiodes (APDs) (Figure 5a, details in the Supporting Information). During these measurements, the number of excitons generated per excitation pulse per PNC, $\langle N \rangle$, was controlled to be below 0.2 by adjusting excitation intensity to evaluate the probability of MX emission.^{33,53,54} Simultaneously, the edge length of individual PNCs was measured by atomic force microscopy (AFM) (see Supporting Information for details).³⁴ Because the PNCs are cubic, the edge length was estimated from the PNC height in the AFM topography images. Samples were prepared by dispersing PNCs on glass coverslips.

Representative photon correlation histograms for single PNCs with $L_{PNC} = 11, 14,$ and 18 nm are shown in Figure 5b. The second-order correlation function at zero-time delay,



Figure 5. (a) Schematic illustration of photon correlation measurements to evaluate the emission photon statistics of single pristine PNCs. (b) Representative photon correlation histograms obtained from single PNCs with $L_{\text{PNC}} = 11$ (left), 14 (middle), and 18 nm (right panel). (c) Relationship between PL peaks, edge lengths (L_{PNC}), and $g^{(2)}(0)$ values obtained from measuring 112 single PNCs.

$g^{(2)}(0)$, was calculated as the ratio of detection events in the central peak to the average in the lateral peaks. Statistically, $g^{(2)}(0) = 0$ when $\langle N_p \rangle = 1$ (ideal single-photon emission), and $g^{(2)}(0) = 0.5$ and 0.67 for $\langle N_p \rangle = 2$ and 3 , respectively. For Poissonian photon emission, $g^{(2)}(0)$ approaches 1. According to Figure 5b, $g^{(2)}(0)$ values of 0.10, 0.37, and 0.81 were obtained for PNCs with $L_{\text{PNC}} = 11$, 14, and 18 nm, respectively, indicating that emission photon statistics shifted from single- to multiphoton as the PNC size increased. Time traces of PL intensity, spectra, correlation histograms, and decay curves for 9 representative PNCs are shown in the Supporting Information. From 112 single PNC measurements, the relationship among the PL peak wavelength, edge length, and $g^{(2)}(0)$ is summarized in Figure 5c. A low $g^{(2)}(0)$ value was preserved near the PL peaks at ~ 530 nm, suggesting that PNCs smaller than ~ 12 nm predominantly exhibited single-photon emission. For PL peaks longer than 530 nm ($L_{\text{PNC}} > 12$ nm), $g^{(2)}(0)$ gradually increased with size, indicating a higher probability of multiphoton emission. These results suggest that longer MX lifetimes in larger PNCs arise from reduced AR rates, which were evaluated by femtosecond transient

absorption measurements (details in the Supporting Information).

Confirmation of Multiple Cy3 Adsorption onto a Single PNC. To enable ET from MX in the PNCs to multiple Cy3 dyes, the adsorption of multiple Cy3 molecules onto a single PNC is necessary. This was confirmed by observing photon correlations from Cy3 PL on single PNCs by exciting Cy3 selectively (Figure 6a, details in the Supporting

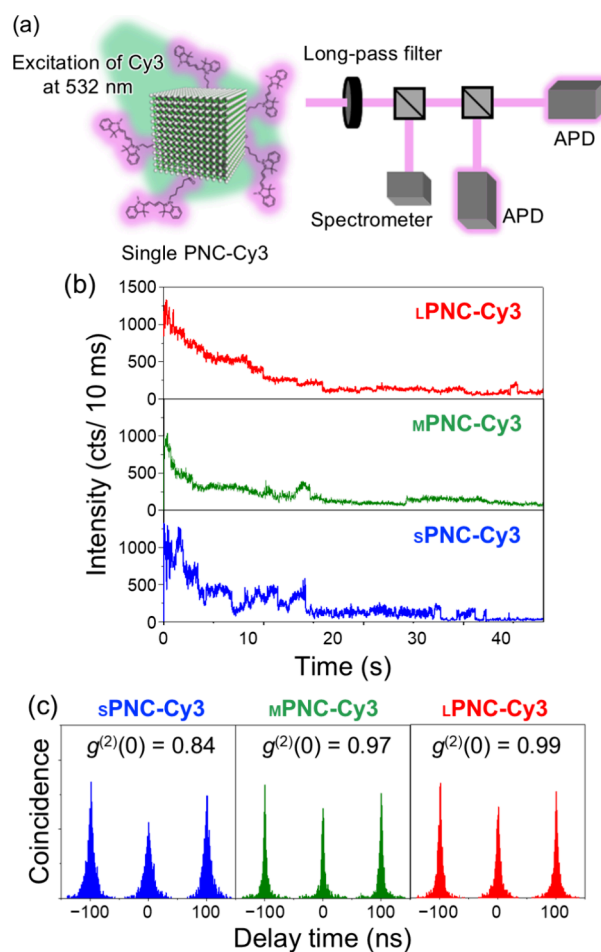


Figure 6. (a) Schematic illustration of PL detection to evaluate the emission photon statistics of Cy3 adsorbed on a single PNC. (b) PL time traces of Cy3 in single sPNC-Cy3 (top panel), mPNC-Cy3 (middle panel), and lPNC-Cy3 (bottom panel). (c) Photon correlation histograms for single sPNC-Cy3 (left panel), mPNC-Cy3 (middle panel), and lPNC-Cy3 (right panel).

Information). $[\text{Cy3}]/[\text{PNC}]$ was varied between 10–15 to maximize the PL intensity of Cy3. Then, the PNC-Cy3 systems were dispersed in PMMA films to increase the survival time of Cy3 and used for the measurement (details in the Supporting Information). In this measurement, an AFM observation was not employed. Representative PL time traces and photon correlation histograms observed from Cy3 on single sPNC, mPNC, and lPNC are shown in Figure 6b,c. The PL intensity degraded stepwise with the measurement time, indicating that multiple Cy3 molecules gradually photobleached.⁵² The photon correlation histograms showed $g^{(2)}(0)$ values close to 1 for all PNC sizes, consistent with the multiphoton emission from multiple Cy3 dyes in each system. These results collectively confirm that multiple Cy3

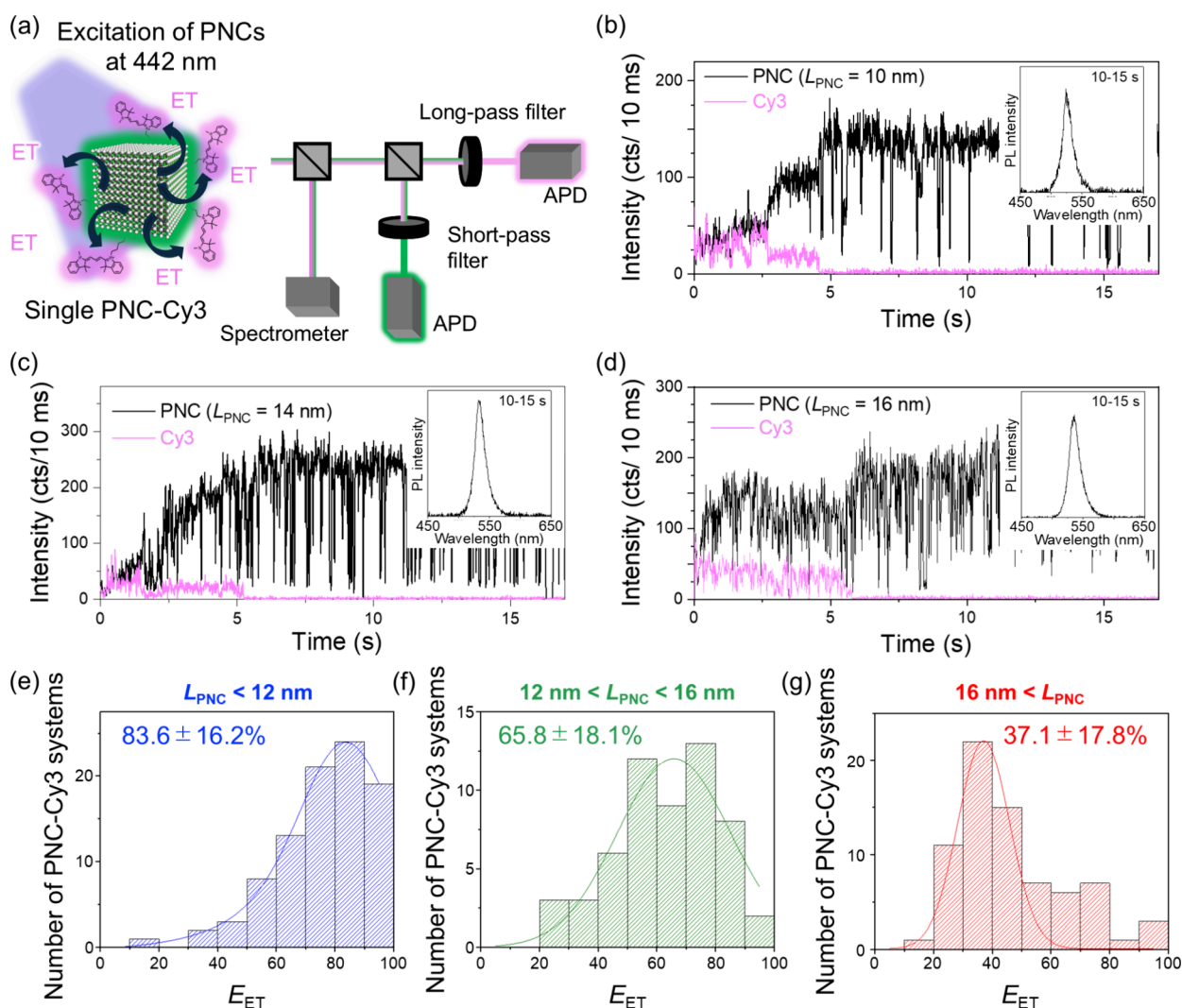


Figure 7. (a) Schematic illustration of PL detection used to evaluate ET from PNCs to Cy3 at the single PNC-Cy3 level. (b–d) Time traces of PL intensity from single PNCs (black line) and Cy3 (pink lines) adsorbed onto PNCs with $L_{\text{PNC}} = 10$ (b), 14 (c), and 16 nm (d). Insets show PL spectra obtained during 10–15 s in each time trace. (e–g) Histograms of E_{ET} values estimated from single PNC-Cy3 systems with different PNC sizes.

molecules were adsorbed onto individual PNCs. Additional data are provided in Figures S21–S29.

Evaluation of ET at the Single PNC-Cy3 Level. To evaluate the ET from the PNCs to Cy3, the PL from Cy3 and the PNCs in single PNC-Cy3 systems were observed simultaneously by exciting PNCs at 442 nm irradiation (Figure 7a, details in the Supporting Information). In this measurement, the PNC-Cy3 systems were dispersed in PMMA films to increase the survival time of Cy3. Thus, as the AFM observation was not employed, the size of the PNC was estimated from the PL peak of the single PNCs using the correlation shown in Figure 5. Initially, PL images of the same area were taken with and without a long-pass filter, which passes only the PL from Cy3 (Figure S30). PL from PNCs and Cy3 can be detected without the long-pass filter, whereas only PL from Cy3 can be detected with the filter. In the images, the positions of the PL spots were consistent, suggesting that the PNCs and Cy3 coexisted and the ET from the PNCs to Cy3 occurred at the single PNC level. By selecting one PL spot, PL from the PNC and Cy3 were measured.

Representative time traces of PL intensity and PL spectra detected from single PNC-Cy3 are shown in Figure 7b–d. From the PL peak, the sizes of the three PNCs were estimated to be 10, 12, and 18 nm, respectively. In all traces, the PL from Cy3 was predominant immediately after the start of the measurement, whereas the PL from the PNCs was quenched. Subsequently, a stepwise decrease in the PL intensity of Cy3 was observed with a stepwise increase in the PL intensity of the PNC. Subsequently, when the PL from Cy3 was dropped to the background count, the PL intensity from the PNCs became the maximum. These observations strongly suggest the ET from the PNCs to Cy3.^{48,52} Other results are shown in Figures S31–S38. By using eq 1, E_{ET} at the single PNC-Cy3 level was estimated and summarized in Figure 7e–g. I and I_0 values are estimated as the most quenched PL intensity and maximum PL intensity of the PNC in the time trace, respectively. PNC-Cy3 systems were separated into 3 groups based on PNCs' size; the first group: $L_{\text{PNC}} < 12$ nm, the second group: $12 \text{ nm} < L_{\text{PNC}} < 16$ nm, and the third group: $16 \text{ nm} < L_{\text{PNC}}$. The average E_{ET} was $83.6 \pm 16.2\%$ for the PNCs with $L_{\text{PNC}} < 12$ nm, $65.8 \pm 18.1\%$ for $12 \text{ nm} < L_{\text{PNC}} < 16$ nm, and $37.1 \pm 17.8\%$ for $16 \text{ nm} < L_{\text{PNC}}$.

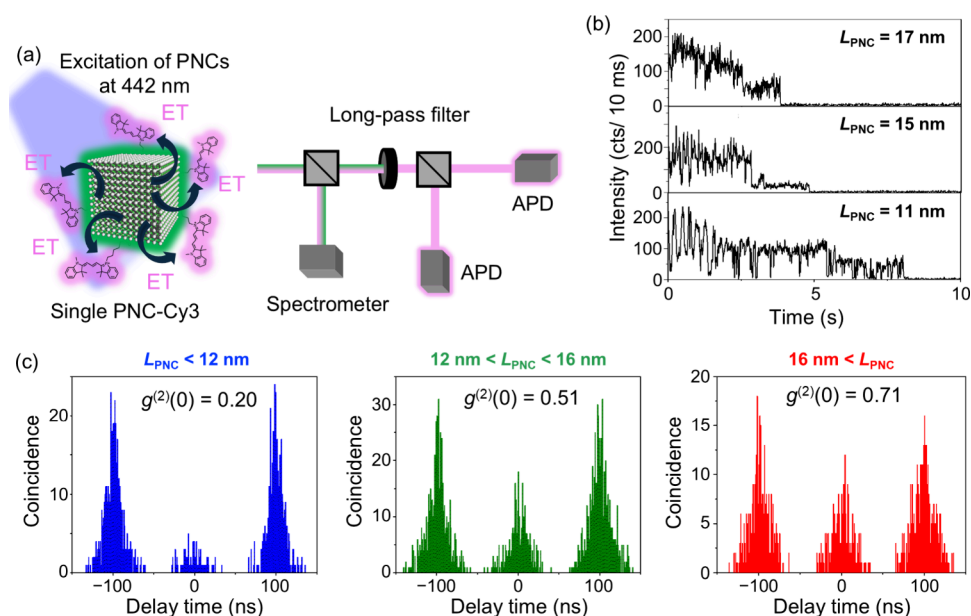


Figure 8. (a) Schematic illustration of the PL detection setup to evaluate the emission photon statistics of Cy3 at the single PNC-Cy3 level. (b) Time traces of PL from Cy3 adsorbed onto single PNCs with $L_{PNC} = 11$ (bottom), 15 (middle), and 17 nm (top) (b). (c) Photon correlation histograms constructed from the PL of Cy3 on single PNCs grouped by size: $L_{PNC} < 12$ nm (left panel), $12\text{--}16$ nm (middle panel), and >16 nm (right panel).

$< L_{PNC}$, respectively. The ET efficiency became higher for the PNC with the smaller size, which was in accordance with that in the solutions (Figure 4).

Evaluation of ET from MX in PNCs to Cy3. Finally, to evaluate ET from MX in PNCs to Cy3, the PL photon statistics of Cy3 via ET were investigated at the single PNC-Cy3 level by using the setup illustrated in Figure 8a. The PL from Cy3 was detected by two APDs through a long-pass filter while exciting the PNCs at 442 nm, where Cy3 exhibits negligible absorption compared to the PNCs. Representative PL intensity traces from PNC-Cy3 systems with $L_{PNC} = 11$, 15, and 17 nm are shown in Figure 8b (additional data are presented in the Supporting Information). In each case, the PL intensity of Cy3 exhibited stepwise decreases and eventually dropped to background levels within 15 s, indicating that multiple Cy3 molecules were adsorbed onto each PNC and emitted via FRET. To elucidate the ET from MX to Cy3, photon correlation histograms of Cy3 were obtained from single PNC-Cy3 systems. Owing to the short survival time of Cy3, histograms shown in Figure 8c were generated by summing the photon correlation data from 9 single PNC-Cy3 systems for $L_{PNC} < 12$ nm, 12 systems for $12 \text{ nm} < L_{PNC} < 16$ nm, and 14 systems for $16 \text{ nm} < L_{PNC}$. The resulting $g^{(2)}(0)$ values were 0.20, 0.51, and 0.71 for $L_{PNC} < 12$ nm, $12 \text{ nm} < L_{PNC} < 16$ nm, and $16 \text{ nm} < L_{PNC}$, respectively, indicating a clear size-dependent trend in PL photon statistics: smaller PNCs favored single-photon emission while larger PNCs led to multiphoton emission from Cy3 via FRET. This trend suggests that in smaller PNCs ($L_{PNC} < 12$ nm), the AR rate is significantly faster than the ET rate, effectively converting MX to SX before FRET occurs. As a result, only one Cy3 molecule is excited via FRET from the SX, resulting in single-photon emission despite the presence of multiple Cy3 molecules. In contrast, larger PNCs ($L_{PNC} > 12$ nm) exhibit slower AR, allowing MX to persist and contribute to FRET, thereby exciting multiple Cy3 molecules and favoring multiphoton emission. These findings are consistent with the size-depend-

ent behavior of MX PL observed in Figure 5. Furthermore, femtosecond transient absorption measurements of the PNCs, as shown in the Supporting Information, revealed that AR became less efficient and its lifetime increased with increasing PNC size. This observation also supports the increase in the efficiency of ET from MX in larger PNCs.

CONCLUSIONS

In this study, we investigated ET from FAPbBr₃ PNCs to Cy3 molecules adsorbed onto the PNCs, with a particular focus on elucidating the possibility of ET from the MX state in a PNC to multiple Cy3 dyes. The FRET from the PNCs to Cy3 was first confirmed at the ensemble level in toluene solution through PL spectra, excitation spectra, and PL lifetime measurements. Subsequently, FRET was evaluated at the single-PNC level by independently detecting the PL from the PNC and Cy3. We demonstrated that ET efficiency strongly depends on the PNC size, which is in agreement with the trend observed in solution-phase measurements. Photon correlation measurements of Cy3 PL via ET from the PNCs revealed insights into the involvement of the MX states. Specifically, Cy3 adsorbed onto PNCs smaller than 12 nm exhibited single-photon emission, suggesting ET predominantly from SX. In contrast, when Cy3 was adsorbed onto PNCs larger than 12 nm, the probability of multiphoton emission from Cy3 increased with increasing PNC size. These results clearly indicate that ET from MX states in PNCs to multiple Cy3 dyes is feasible, demonstrating that MX energy can be efficiently harvested by using PNCs with sizes exceeding 12 nm. In other words, ET from MX can be achieved in larger PNCs, although the ET efficiency decreases. Therefore, we conclude that larger PNCs adsorbing a large number of acceptor molecules, which accelerate ET efficiency, are ideal systems for the efficient utilization of MX in PNCs. Our findings provide key insights into the design of photosensitizer systems based on PNC-organic hybrid materials and photonic applications.

EXPERIMENTAL SECTION

Materials and Methods. *Materials.* All commercially available reagents were reagent grade and used without further purification. The solvents used for measurements were spectral grade and were also used without purification.

General Methods. UV/vis absorption and photoluminescence (PL) spectra were recorded by using a SHIMADZU UV-3600 spectrophotometer and a HITACHI F-7000 spectrophotometer, respectively. Absolute PL quantum yield (PLQY) was measured using a HAMAMATSU Quantaurus-QY Plus C13534-01 with an integrating sphere. Transmission electron microscopy (TEM) imaging was performed using a JEOL JEM-2100F instrument operated at an acceleration voltage of 200 kV. The samples were prepared by spin-coating solutions onto a carbon-coated STEM Cu grid (HRC-C10 STEM Cu100P), followed by drying under a vacuum for 1 h. TEM observations were conducted without staining.

Synthesis and Characterization of FAPbBr₃ PNCs. *Chemicals.* Oleylamine (80–90%) was purchased from Acros Organics. 1-Octadecene (90%), oleic acid (90%), and formamidinium (FA) acetate (99.9%) were purchased from Sigma-Aldrich. Hydrobromic acid (47%) was purchased from the Tokyo Chemical Industry. Lead acetate trihydrate (99.9%), ethanol (99.5%), diethyl ether (99.5%), and toluene (for spectrochemical analysis, 99.8%) were purchased from FUJIFILM Wako. All chemicals were used without further purification.

Synthesis of Oleylamine Bromide. Oleylamine bromide was synthesized according to a previous report.⁹ Oleylamine (12.5 mL) was dissolved in ethanol (100 mL), and the solution was cooled to 0 °C. Hydrobromic acid (47%, 8.6 mL) was added dropwise. The solution was stirred overnight under a N₂ atmosphere. The resulting solution was dried in vacuo to obtain a brown solid, which was then washed with diethyl ether to yield oleylamine bromide.

Syntheses of FAPbBr₃ PNCs. FAPbBr₃ PNCs were synthesized following a previous method with minor modifications.⁹ Lead acetate trihydrate (76 mg), FA acetate (78 mg), oleic acid (2 mL), and 1-octadecene (8 mL) were added to a round-bottom flask. The mixture was stirred at 50 °C under a vacuum for 30 min. After heating to the target temperature (90, 120, and 130 °C for *s*PNC, *m*PNC, and *l*PNC, respectively), a toluene solution (2 mL) containing oleylamine bromide (210 mg) was promptly injected. The resulting mixture was stirred for 10 s and then cooled to below 20 °C in an ice bath to obtain a suspension. For purification of *s*PNC, 10 mL of toluene and 5 mL of acetonitrile were added to the suspension, followed by centrifugation (10,000 rpm/5 min) to collect the precipitates. For *m*PNC and *l*PNC, 10 mL of toluene was added to each suspension and centrifuged (5000 rpm/5 min) to collect the precipitates. The precipitates were redispersed in 10 mL of toluene and centrifuged again (3000 rpm/5 min) to obtain the supernatant containing the PNC solutions. Absorption and PL spectra of the obtained PNCs dispersed in toluene are shown in Figure S1.

Evaluation of PL Behaviors at the Single PNC Level. *Sample Preparation.* For single pristine PNC measurements, the PNCs were dispersed onto a glass coverslip by spin-coating their toluene solution. For single PNC-Cy3 measurements, the PNC-Cy3 systems were dispersed in a poly(methyl methacrylate) (PMMA) thin film on a glass coverslip by spin-coating a PMMA/toluene solution containing PNC-Cy3 systems. A PMMA thin film having a thickness of about 30 nm was formed by spin-coating a 0.5 wt % PMMA/CHCl₃ solution at 3000 rpm. To ensure isolation of single PNC-Cy3 systems within the confocal volume, their density in the PMMA film was maintained below 10 per 10 μm × 10 μm area.

Instrumental Setup. Single PNC-level measurements were performed using a microspectroscopy setup comprising an excitation laser, an inverted microscope (Olympus, IX-71), an atomic force microscope (AFM, Nano Wizard II, JPK Instruments), and a PL detection system. For simultaneous measurement of PNC size and PL behavior, AFM was integrated with the setup. Picosecond-pulsed lasers at 442 and 532 nm (10.0 MHz, 90 ps full width at half-maximum, PicoQuant) were used to excite the PNCs and Cy3 dyes,

respectively. The laser beams were circularly polarized by using a Glan-Thomson polarizer and a λ/4 wave plate. The beam was directed into the inverted microscope and reflected by a dichroic mirror (Chroma, 440DCLP for 442 nm, Semrock, FF555-Di02 for 532 nm) and then focused to a diffraction-limited spot on the sample using an objective lens (Olympus, 100×, NA 1.4). In simultaneous measurements of PNC size and emission behavior, the AFM topography was recorded in tapping mode. The AFM cantilever (Olympus, model OMCL-AC160TS-R3) was aligned with the center of the focused laser. By scanning the sample, we acquired PL images and AFM topography. For other measurements, only PL images were recorded. After image acquisition, an individual PNC or PNC-Cy3 complex was selected, and its PL behavior was monitored under laser excitation. Emitted photons were collected via the same objective lens, passed through a confocal pinhole (100 μm), and filtered using long-pass (LP) filters (Semrock, LP02-458 for 442 nm excitation; FF01-593 for 532 nm excitation) to remove residual excitation light. Half of the collected photons were directed to a spectrometer (Acton Research Corporation, SpectraPro2358) equipped with an air-cooled EMCCD camera (Princeton Instruments, PIXIS400B). The remaining photons were split equally using a 50:50 nonpolarizing beam splitter and directed to two avalanche photodiodes (APDs; PerkinElmer, SPCM-AQR-14). For selective detection of PNCs and Cy3 PL, a short-pass (SP) filter (Semrock, FF01-546/SP-25) and an LP filter (Semrock, FF01-593/LP-25) were used depending on the measurements (Figure S10 in the Supporting Information). For photon correlation measurement of Cy3 in the single PNC-Cy3 systems, the LP filter was put in front of the beam splitter cube (Figures 6a and 8a). For the evaluation of the ET in the single PNC-Cy3 systems, the SP filter was put in front of one APD, and the LP filter was put in front of the other APD (Figure 7a). The signals from both APDs were connected to the router of a time-correlated single-photon counting (TCSPC) PC board (Becker & Hickl, SPC630) to measure the PL lifetime and to collect data for the photon correlation histogram. The signal from one of the two APDs was delayed using a delay generator (Stanford Research, DG535) to compensate for the dead time of the TCSPC board. Time-resolved data were acquired using a first-in-first-out mode, in which the arrival time after the beginning of the acquisition, the time delay between the start and stop pulses, and the detection channel were registered for each detected PL photon. The data were analyzed using a homemade LabVIEW routine that allowed for the simultaneous measurement of the time trace of PL intensity, PL lifetime, and the photon correlation histogram. All measurements were conducted under ambient conditions (22 °C and 20–35% relative humidity).

Evaluation of Emission Photon Statistics of Single Pristine PNCs. The emission photon statistics from single pristine PNCs were observed under 442 nm excitation, as illustrated in Figure 5a. The AFM topography image and PL image of single PNCs in the same area were obtained by scanning the sample. Time traces of PL intensity, PL spectra, and photon correlation histograms for single PNCs were subsequently measured.

Confirmation of Adsorption of Multiple Cy3 Dyes onto Single PNC. To verify the adsorption of multiple Cy3 dye molecules onto individual PNCs, photon correlation measurements were conducted by selectively exciting Cy3 with a 532 nm laser beam, as illustrated in Figure 6a.

Evaluation of ET from PNCs to Cy3 at the Single PNC-Cy3 Level. The ET from PNCs to adsorbed Cy3 at the single PNC-Cy3 level was monitored by selectively exciting the PNCs at 442 nm. PL from the PNCs and Cy3 was detected simultaneously using two APDs with SP and LP filters, as illustrated in Figure 7a.

Evaluation of ET from MX in a Single PNC to Multiple Cy3 Dyes. To evaluate ET from MX in the PNCs to multiple Cy3 molecules adsorbed on the PNC surfaces, PL photon statistics of Cy3 in the PNC-Cy3 systems were analyzed at the single PNC-Cy3 level by 442 nm excitation. The PL from Cy3, resulting from FRET from the PNCs, was detected by two APDs through an LP filter, as illustrated in Figure 8a.

■ ASSOCIATED CONTENT

SI Supporting Information

The Supporting Information is available free of charge at <https://pubs.acs.org/doi/10.1021/jacs.5c11022>.

Absorption and PL spectra of PNCs dispersed in toluene, estimation of Auger recombination rate, Estimation of molar absorption coefficient of the PNC, calculation of the energy transfer efficiency, PL spectra of PNC-Cy3 systems dispersed in toluene, excitation spectra of PNC-Cy3 systems dispersed in toluene, PL decay curves of PNC-Cy3 systems dispersed in toluene, transmission spectra of short-pass and long-pass filters, evaluation of emission photon statistics of the single pristine PNCs, confirmation of adsorption of multiple Cy3 dyes onto single PNCs, evaluation of ET from PNCs to Cy3 at the single PNC-Cy3 levels, and evaluation of ET from MX in a single PNC to multiple Cy3 dyes (PDF)

■ AUTHOR INFORMATION

Corresponding Author

Sadahiro Masuo – Department of Applied Chemistry for Environment, Kwansei Gakuin University, Sanda, Hyogo 669-1330, Japan; orcid.org/0000-0003-4828-5968; Email: masuo@kwansei.ac.jp

Authors

Tetsuo Yamaguchi – Department of Applied Chemistry for Environment, Kwansei Gakuin University, Sanda, Hyogo 669-1330, Japan; orcid.org/0000-0002-6697-2916

Tomoya Fukumasu – Department of Applied Chemistry for Environment, Kwansei Gakuin University, Sanda, Hyogo 669-1330, Japan

Yukihide Ishibashi – Department of Applied Chemistry, Graduate School of Science and Engineering, Ehime University, Matsuyama, Ehime 790-8577, Japan; orcid.org/0000-0002-4015-8828

Complete contact information is available at: <https://pubs.acs.org/doi/10.1021/jacs.5c11022>

Notes

The authors declare no competing financial interest.

■ ACKNOWLEDGMENTS

This work was financially supported by KAKENHI grant numbers 23K21106, 24K23091, and 25K01747 from the Japan Society for the Promotion of Science (JSPS), and by JSPS KAKENHI grant number 23H04875 in a Grant-in-Aid for Transformative Research Areas “Materials Science of Meso-Hierarchy”. TEM measurements were supported by the Advanced Research Infrastructure for Materials and Nanotechnology (JPMXP1224MS1005) of MEXT, Institute for Molecular Science, Instrument Center, Okazaki, Japan.

■ REFERENCES

- (1) Brus, L. E. A simple model for the ionization potential, electron affinity, and aqueous redox potentials of small semiconductor crystallites. *J. Chem. Phys.* **1983**, *79* (11), 5566–5571.
- (2) Bawendi, M. G.; Steigerwald, M. L.; Brus, L. E. The Quantum Mechanics of Larger Semiconductor Clusters (“Quantum Dots”). *Annu. Rev. Phys. Chem.* **1990**, *41* (1), 477–496.
- (3) Murray, C. B.; Norris, D. J.; Bawendi, M. G. Synthesis and Characterization of Nearly Monodisperse CdE (E = S, Se, Te) Semiconductor Nanocrystallites. *J. Am. Chem. Soc.* **1993**, *115*, 8706–8715.
- (4) Alivisatos, A. P. Semiconductor Clusters, Nanocrystals, and Quantum Dots. *Science* **1996**, *271*, 933–937.
- (5) Talapin, D. V.; Lee, J.-S.; Kovalenko, M. V.; Shevchenko, E. V. Prospects of Colloidal Nanocrystals for Electronic and Optoelectronic Applications. *Chem. Rev.* **2010**, *110* (1), 389–458.
- (6) Schmidt, L. C.; Pertegas, A.; Gonzalez-Carrero, S.; Malinkiewicz, O.; Agouram, S.; Minguez Espallargas, G.; Bolink, H. J.; Galian, R. E.; Perez-Prieto, J. Nontemplate synthesis of CH₃NH₃PbBr₃ perovskite nanoparticles. *J. Am. Chem. Soc.* **2014**, *136* (3), 850–853.
- (7) Protesescu, L.; Yakunin, S.; Bodnarchuk, M. I.; Krieg, F.; Caputo, R.; Hendon, C. H.; Yang, R. X.; Walsh, A.; Kovalenko, M. V. Nanocrystals of Cesium Lead Halide Perovskites (CsPbX₃, X = Cl, Br, and I): Novel Optoelectronic Materials Showing Bright Emission with Wide Color Gamut. *Nano Lett.* **2015**, *15* (6), 3692–3696.
- (8) Akkerman, Q. A.; D’Innocenzo, V.; Accornero, S.; Scarpellini, A.; Petrozza, A.; Prato, M.; Manna, L. Tuning the Optical Properties of Cesium Lead Halide Perovskite Nanocrystals by Anion Exchange Reactions. *J. Am. Chem. Soc.* **2015**, *137* (32), 10276–10281.
- (9) Protesescu, L.; Yakunin, S.; Bodnarchuk, M. I.; Bertolotti, F.; Masciocchi, N.; Guagliardi, A.; Kovalenko, M. V. Monodisperse Formamidinium Lead Bromide Nanocrystals with Bright and Stable Green Photoluminescence. *J. Am. Chem. Soc.* **2016**, *138* (43), 14202–14205.
- (10) Kovalenko, M. V.; Protesescu, L.; Bodnarchuk, M. I. Properties and potential optoelectronic applications of lead halide perovskite nanocrystals. *Science* **2017**, *358* (6364), 745–750.
- (11) Klimov, V. I.; Ivanov, S. A.; Nanda, J.; Achermann, M.; Bezel, I.; McGuire, J. A.; Piryatinski, A. Single-exciton optical gain in semiconductor nanocrystals. *Nature* **2007**, *447* (7143), 441–446.
- (12) Nozik, A. J.; Beard, M. C.; Luther, J. M.; Law, M.; Ellingson, R. J.; Johnson, J. C. Semiconductor Quantum Dots and Quantum Dot Arrays and Applications of Multiple Exciton Generation to Third-Generation Photovoltaic Solar Cells. *Chem. Rev.* **2010**, *110*, 6873–6890.
- (13) Sambur, J. B.; Novet, T.; Parkinson, B. A. Multiple Exciton Collection in a Sensitized Photovoltaic System. *Science* **2010**, *330*, 63–66.
- (14) Yakunin, S.; Protesescu, L.; Krieg, F.; Bodnarchuk, M. I.; Nedelcu, G.; Humer, M.; De Luca, G.; Fiebig, M.; Heiss, W.; Kovalenko, M. V. Low-threshold amplified spontaneous emission and lasing from colloidal nanocrystals of caesium lead halide perovskites. *Nat. Commun.* **2015**, *6*, 8056.
- (15) Pietryga, J. M.; Park, Y. S.; Lim, J.; Fidler, A. F.; Bae, W. K.; Brovelli, S.; Klimov, V. I. Spectroscopic and Device Aspects of Nanocrystal Quantum Dots. *Chem. Rev.* **2016**, *116*, 10513–10622.
- (16) Kazes, M.; Nakar, D.; Cherniukh, I.; Bodnarchuk, M. I.; Feld, L. G.; Zhu, C.; Amgar, D.; Raino, G.; Kovalenko, M. V.; Oron, D. Observation of Three-Photon Cascaded Emission from Triexcitons in Giant CsPbBr₃ Quantum Dots at Room Temperature. *Nano Lett.* **2024**, *24* (42), 13185–13191.
- (17) Benson, O.; Santori, C.; Pelton, M.; Yamamoto, Y. Regulated and Entangled Photons from a Single Quantum Dot. *Phys. Rev. Lett.* **2000**, *84*, 2513.
- (18) Klimov, V. I.; Mikhailovsky, A. A.; McBranch, D. W.; Leatherdale, C. A.; Bawendi, M. G. Quantization of Multiparticle Auger Rates in Semiconductor Quantum Dots. *Science* **2000**, *287* (5455), 1011–1013.
- (19) Fisher, B.; Caruge, J. M.; Zehnder, D.; Bawendi, M. Room-Temperature Ordered Photon Emission from Multiexciton States in Single CdSe Core-Shell Nanocrystals. *Phys. Rev. Lett.* **2005**, *94*, No. 087403.
- (20) Klimov, V. I. Spectral and dynamical properties of multiexcitons in semiconductor nanocrystals. *Annu. Rev. Phys. Chem.* **2007**, *58*, 635–673.

- (21) Klimov, V. I. Multicarrier Interactions in Semiconductor Nanocrystals in Relation to the Phenomena of Auger Recombination and Carrier Multiplication. *Annu. Rev. Condens. Matter Phys.* **2014**, *4*, 285–316.
- (22) Melnychuk, C.; Guyot-Sionnest, P. Multicarrier Dynamics in Quantum Dots. *Chem. Rev.* **2021**, *121*, 2325–2372.
- (23) Nirmal, M.; Dabbousi, B. O.; Bawendi, M. G.; Macklin, J. J.; Trautman, J. K.; Harris, T. D.; Brus, L. E. Fluorescence Intermittency in Single Cadmium Selenide Nanocrystals. *Nature* **1996**, *383*, 802–804.
- (24) Efros, A. L.; Rosen, M. Random Telegraph Signal in the Photoluminescence Intensity of a Single Quantum Dot. *Phys. Rev. Lett.* **1997**, *78*, 1110.
- (25) Nirmal, M.; Brus, L. Luminescence Photophysics in Semiconductor Nanocrystals. *Acc. Chem. Res.* **1999**, *32* (5), 407–414.
- (26) Efros, A. L.; Nesbitt, D. J. Origin and Control of Blinking in Quantum Dots. *Nat. Nanotechnol.* **2016**, *11*, 661–671.
- (27) Robel, I.; Gresback, R.; Kortshagen, U.; Schaller, R. D.; Klimov, V. I. Universal Size-dependent Trend in Auger Recombination in Direct-gap and Indirect-gap Semiconductor Nanocrystals. *Phys. Rev. Lett.* **2009**, *102*, No. 177404.
- (28) Castaneda, J. A.; Nagamine, G.; Yassitepe, E.; Bonato, L. G.; Voznyy, O.; Hoogland, S.; Nogueira, A. F.; Sargent, E. H.; Cruz, C. H. B.; Padilha, L. A. Efficient Biexciton Interaction in Perovskite Quantum Dots Under Weak and Strong Confinement. *ACS Nano* **2016**, *10*, 8603–8609.
- (29) Makarov, N. S.; Guo, S. J.; Isaienko, O.; Liu, W. Y.; Robel, I.; Klimov, V. I. Spectral and Dynamical Properties of Single Excitons, Biexcitons, and Triions in Cesium-Lead-Halide Perovskite Quantum Dots. *Nano Lett.* **2016**, *16*, 2349–2362.
- (30) Li, Y.; Luo, X.; Ding, T.; Lu, X.; Wu, K. Size- and Halide-Dependent Auger Recombination in Lead Halide Perovskite Nanocrystals. *Angew. Chem., Int. Ed.* **2020**, *59*, 14292–14295.
- (31) Chen, Y.; Vela, J.; Htoon, H.; Casson, J. L.; Werder, D. J.; Bussiah, D. A.; Klimov, V. I.; Hollingsworth, J. A. “Giant” Multishell CdSe Nanocrystal Quantum Dots with Suppressed Blinking. *J. Am. Chem. Soc.* **2008**, *130* (15), 5026–5027.
- (32) García-Santamaría, F.; Brovelli, S.; Viswanatha, R.; Hollingsworth, J. A.; Htoon, H.; Crooker, S. A.; Klimov, V. I. Breakdown of Volume Scaling in Auger Recombination in CdSe/CdS Heteronanocrystals: The Role of the Core–Shell Interface. *Nano Lett.* **2011**, *11*, 687–693.
- (33) Park, Y. S.; Bae, W. K.; Padilha, L. A.; Pietryga, J. M.; Klimov, V. I. Effect of the Core/Shell Interface on Auger Recombination Evaluated by Single-Quantum-Dot Spectroscopy. *Nano Lett.* **2014**, *14*, 396–402.
- (34) Igarashi, H.; Yamauchi, M.; Masuo, S. Correlation between Single-Photon Emission and Size of Cesium Lead Bromide Perovskite Nanocrystals. *J. Phys. Chem. Lett.* **2023**, *14* (9), 2441–2447.
- (35) Leblanc, S. J.; McClanahan, M. R.; Jones, M.; Moyer, P. J. Enhancement of Multiphoton Emission from Single CdSe Quantum Dots Coupled to Gold Films. *Nano Lett.* **2013**, *13*, 1662–1669.
- (36) Park, Y.-S.; Ghosh, Y.; Chen, Y.; Piryatinski, A.; Xu, P.; Mack, N. H.; Wang, H.-L.; Klimov, V. I.; Hollingsworth, J. A.; Htoon, H. Super-Poissonian Statistics of Photon Emission from Single CdSe-CdS Core-Shell Nanocrystals Coupled to Metal Nanostructures. *Phys. Rev. Lett.* **2013**, *110*, No. 117401.
- (37) Dey, S.; Zhao, J. Plasmonic Effect on Exciton and Multiexciton Emission of Single Quantum Dots. *J. Phys. Chem. Lett.* **2016**, *7*, 2921–2929.
- (38) Dey, S.; Zhou, Y.; Sun, Y.; Jenkins, J. A.; Kriz, D.; Suib, S. L.; Chen, O.; Zou, S.; Zhao, J. Excitation Wavelength Dependent Photon Anti-bunching/Bunching from Single Quantum Dots near Gold Nanostructures. *Nanoscale* **2018**, *10*, 1038–1046.
- (39) Masuo, S.; Kanetaka, K.; Sato, R.; Teranishi, T. Direct Observation of Multiphoton Emission Enhancement from a Single Quantum Dot Using AFM Manipulation of a Cubic Gold Nanoparticle. *ACS Photonics* **2016**, *3*, 109–116.
- (40) Takata, H.; Naiki, H.; Wang, L.; Fujiwara, H.; Sasaki, K.; Tamai, N.; Masuo, S. Detailed Observation of Multiphoton Emission Enhancement from a Single Colloidal Quantum Dot Using a Silver-Coated AFM Tip. *Nano Lett.* **2016**, *16*, 5770–5778.
- (41) Masuo, S.; Naiki, H.; Machida, S.; Itaya, A. Photon statistics in enhanced fluorescence from a single CdSe/ZnS quantum dot in the vicinity of silver nanoparticles. *Appl. Phys. Lett.* **2009**, *95* (19), 193106.
- (42) Naiki, H.; Masuo, S.; Machida, S.; Itaya, A. Single-Photon Emission Behavior of Isolated CdSe/ZnS Quantum Dots Interacting with the Localized Surface Plasmon Resonance of Silver Nanoparticles. *J. Phys. Chem. C* **2011**, *115* (47), 23299–23304.
- (43) Naiki, H.; Uedao, T.; Wang, L.; Tamai, N.; Masuo, S. Multiphoton Emission Enhancement from a Single Colloidal Quantum Dot Using SiO₂-Coated Silver Nanoparticles. *ACS Omega* **2017**, *2* (2), 728–737.
- (44) Dayal, S.; Burda, C. One- and Two-photon Induced QD-Based Energy Transfer and the Influence of Multiple QD Excitations. *Photochem. Photobiol. Sci.* **2008**, *7*, 605–613.
- (45) Xiao, J.; Wang, Y.; Hua, Z.; Wang, X.; Zhang, C.; Xiao, M. Carrier Multiplication in Semiconductor Nanocrystals Detected by Energy Transfer to Organic Dye Molecules. *Nat. Commun.* **2012**, *3*, 1170.
- (46) Huang, X. N.; Xu, Q. F.; Zhang, C. F.; Wang, X. Y.; Xiao, M. Energy Transfer of Biexcitons in a Single Semiconductor Nanocrystal. *Nano Lett.* **2016**, *16*, 2492–2496.
- (47) Li, B.; Liu, Y.; Wan, Y.; Zhu, L.; Shi, Y.; Liu, C.; Jin, M.; Gao, J.; Ding, D. Forster Resonance Energy Transfer Outpaces Auger Recombination in CdTe/CdS Quantum Dots-Rhodamine101 Molecules System upon Compression. *Opt. Express* **2021**, *29*, 27171–27180.
- (48) Yoshioka, M.; Yamauchi, M.; Tamai, N.; Masuo, S. Single-Photon Emission from Organic Dye Molecules Adsorbed on a Quantum Dot via Energy Transfer. *Nano Lett.* **2023**, *23* (24), 11548–11554.
- (49) Hofmann, F. J.; Bodnarchuk, M. I.; Dirin, D. N.; Vogelsang, J.; Kovalenko, M. V.; Lupton, J. M. Energy Transfer from Perovskite Nanocrystals to Dye Molecules Does Not Occur by FRET. *Nano Lett.* **2019**, *19*, 8896–8902.
- (50) Hofmann, F. J.; Bodnarchuk, M. I.; Protesescu, L.; Kovalenko, M. V.; Lupton, J. M.; Vogelsang, J. Exciton Gating and Triplet Deshelling in Single Dye Molecules Excited by Perovskite Nanocrystal FRET Antennae. *J. Phys. Chem. Lett.* **2019**, *10*, 1055–1062.
- (51) Cho, K.; Yamada, T.; Tahara, H.; Tadano, T.; Suzuura, H.; Saruyama, M.; Sato, R.; Teranishi, T.; Kanemitsu, Y. Luminescence Fine Structures in Single Lead Halide Perovskite Nanocrystals: Size Dependence of the Exciton–Phonon Coupling. *Nano Lett.* **2021**, *21* (17), 7206–7212.
- (52) Matsunaga, K.; Inoue, I.; Koyama, S.; Yamaguchi, T.; Yamauchi, M.; Masuo, S. Energy Transfer from a Perovskite Nanocrystal to Cyanine Dyes Depending on Spectral Overlap Revealed by a Single-Particle Spectroscopy. *Nano Lett.* **2025**, *25* (15), 6145–6151.
- (53) Park, Y. S.; Malko, A. V.; Vela, J.; Chen, Y.; Ghosh, Y.; Garcia-Santamaría, F.; Hollingsworth, J. A.; Klimov, V. I.; Htoon, H. Near-unity quantum yields of biexciton emission from CdSe/CdS nanocrystals measured using single-particle spectroscopy. *Phys. Rev. Lett.* **2011**, *106* (18), No. 187401.
- (54) Nair, G.; Zhao, J.; Bawendi, M. G. Biexciton quantum yield of single semiconductor nanocrystals from photon statistics. *Nano Lett.* **2011**, *11* (3), 1136–1140.